HHS Public Access

Author manuscript

ASAIO J. Author manuscript; available in PMC 2024 August 01.

Published in final edited form as:

ASAIO J. 2023 August 01; 69(8): 756–765. doi:10.1097/MAT.0000000000001948.

Application of 1000 fps high-speed angiography to in-vitro hemodynamic evaluation of left ventricular assist device outflow graft configurations

Allison Shields[1,2], **Swetadri Vasan Setlur Nagesh**[1,2], **Keshava Rajagopal**[3], **Daniel R. Bednarek**[1,2], **Stephen Rudin**[1,2], **Venkat Keshav Chivukula**[4]

[1]Medical Physics Program, University at Buffalo, Buffalo, New York, USA

[2]Canon Stroke and Vascular Research Center, University at Buffalo, Buffalo, New York, USA

[3]Division of Cardiac Surgery, Department of Surgery, Sidney Kimmel Medical College, Thomas Jefferson University, Philadelphia, Pennsylvania, USA

[4]Department of Biomedical Engineering, Florida Institute of Technology, Melbourne, Florida, USA

Abstract

Left-ventricular assist device (LVAD)-induced hemodynamics are characterized by fast moving flow with large variations in velocity, making quantitative assessments difficult with existing imaging methods. This study demonstrates the ability of 1000 fps high-speed angiography (HSA) to quantify the effect of the surgical implantation angle of a LVAD outflow graft on the hemodynamics within the ascending aorta in-vitro. HSA was performed on patient-derived, 3D-printed optically opaque aortic models using a non-soluble contrast media, Ethiodol, as a flow tracer. Outflow graft configuration angles of 45- and 90-degrees with respect to the central aortic axis were considered. Projected velocity distributions were calculated from the high-speed experimental sequences using two methods: a physics-based optical flow algorithm and tracking of radio-opaque particles. Particle trajectories were also used to evaluate accumulated shear stress. Results were then compared with computational fluid dynamics (CFD) simulations to confirm the results of the high-speed imaging method. Flow patterns derived from HSA coincided with the impingement regions and recirculation zones formed in the aortic root as seen in the CFD for both graft configurations. Compared to the 45-degree graft, the 90-degree configuration resulted in 81% higher 2D-projected velocities (over 100 cm/s) along the contralateral wall of the aorta. Both graft configurations suggest elevated accumulated shear stresses along individual trajectories. Compared to CFD simulations, HSA successfully characterized the fast-moving flow and hemodynamics in each LVAD graft configuration in-vitro, demonstrating the potential utility of this technology as a quantitative imaging modality.

Address for Correspondence: Venkat Keshav Chivukula, 150 W University Blvd, Florida Institute of Technology, Melbourne, FL 32901, 321-674-7311, vchivukula@fit.edu.

Conflicts of Interest: None

Keywords

High-Speed Angiography; Left-Ventricular Assist Device; Stroke; Computational Fluid Dynamics; Heart Failure

Introduction

Hemodynamic information plays a critical role in the diagnosis and treatment of vascular disease.[1, 2] Standard planar angiography involves the injection of an iodine-based contrast agent, and a sequence of x-ray images are taken to evaluate the flow of contrast as it is propagated throughout the vascular network. It is possible to glean some dynamic flow information from these sequences, but detailed analysis of hemodynamics is not routinely performed. Computational fluid dynamics (CFD) simulations are useful in that they yield high-resolution, volumetric flow information, but remain lacking in their real-time implementation and adherence to true in-vivo flow boundary conditions. Therefore, it is of interest to bridge the gap between quantitative hemodynamic analysis and diagnostic imaging across a number of clinical indications.

In the cardiovascular space, quantitative flow analysis is especially difficult, even under normal physiologic conditions: high arterial flow rates, patient motion, and suboptimal temporal resolution of existing imaging modalities are all contributing factors. The addition of mechanical circulatory support devices further complicates the problem. For end-stage heart failure (HF) patients, the decision to proceed with a left ventricular assist device (LVAD) as a bridge to transplantation or destination therapy may be a viable option, depending on the patient's projected waiting time to transplantation and degree of hemodynamic compromise. The implantation rate of LVADs continues to grow, with over half of cases indicated as destination therapy; however, LVAD patients continue to remain at risk for devastating neurologic events such as stroke, which severely limit long-term outcomes.[3, 4] The incidence of stroke with continuous-flow LVAD implantation is 10% in the first year alone along with a variety of other hemodynamic complications, indicating the current clinical need for improving hemodynamic performance and outcomes of LVAD therapy.[5–7]

The nuances of surgical outflow graft implantation configuration may further exacerbate unfavorable hemodynamics resulting from LVAD implantation.[8–10] High-spatiotemporal resolution is necessary to quantify the rapid flow present in the aortic arch, due to the disruptive flow patterns resulting from the LVAD outflow graft as well as the complex geometry of the arch itself. Therefore, the majority of quantitative assessment of these adverse flow patterns comes from computational fluid dynamics (CFD) simulations.[9, 11, 12] There is a distinct lack of in-vivo, or even in-vitro assessments, chiefly due to the nature of the problem: the flow exiting the outflow cannula is high speed (>100 cm/s). CT and echocardiography may be used for post procedure follow-up[13, 14], but direct visualization of flow is limited in the surgical suite to ultrasound or coronary angiography. Despite these difficulties, research has shown that quantitative hemodynamic metrics are

potentially indicative of the long-term success of the LVAD implantation and likelihood of complications such as thrombosis.[8]

To that end, we introduce the use of novel high-speed x-ray detector technology, which would enable determinations of detailed blood flow distributions. The high-speed angiographic (HSA) system is based on the use of low-noise, photon-counting x-ray detectors, which enable imaging at an unprecedented temporal resolution of 1000 fps.[15] In this work, the high-speed method is applied to optically-opaque 3D-printed vascular LVAD models: for the first time, angiographic imaging is able to directly quantify known hemodynamic phenomena as a result of the LVAD graft anastomosis angle. Two surgically relevant LVAD outflow graft configurations are presented. Quantitative HSA-derived results are then compared with CFD simulations, the widely accepted standard of estimating detailed flow characteristics in LVAD's.

Methods

Test Bench Setup

To replicate physiologic flow conditions in-vitro, a 3D model was constructed from CTA-derived patient-specific vasculature (Solidworks, Dassault Systems, France) of the ascending aorta and great vessel bifurcations.[9] The vessel lumen was exported in stereolithographic (STL) format, and a 10-mm diameter LVAD outflow graft was digitally anastomosed to the ascending aorta, distal to the aortic root and proximal to the brachiocephalic artery via virtual surgery.[9, 11] Two clinically-relevant outflow graft configurations were evaluated, at 45- and 90-degrees with respect to the central axis of the ascending aorta (Figure 1). Both the outflow graft and aortic arch were assumed to be rigid and 3D-printed in optically opaque polylactic acid (PLA) filament (Creality 3D, Shenzhen, China). The aortic root region was slightly extended for the in-vitro flow experiments with a cap to seal off flow that would be entering from the aortic valve: the native left ventricular contractility and flow through the aortic valve was assumed to be negligible, representing full LVAD support. Each LVAD model was connected to a flow loop (Figure 2), with the pump (CompuFlow 1000 MR, Shelley Medical Imaging Technologies, London, ON) programmed to achieve a constant 5 L/min flow rate at the outflow graft. A 60%−40% water-glycerol mixture by volume was used as a blood-analog fluid and heated to 37-degrees Celsius to replicate the approximate viscosity of blood. A flow transducer (Hugo Sachs Elektronik, Model 79232, Germany) was used to verify the inlet boundary conditions, which were then used in the CFD simulation. Mechanical clamps were used to control the flow more finely through the outlets, to achieve a physiologic flow split of approximately 60% of flow through the descending aorta and 40% through the ascending vessels (approximate flow splits are as follows: 20% brachiocephalic, 10% common carotid, 10% left subclavian).

Imaging Setup

The Aries detector (Direct Conversion-Varex Inc., Sweden) was utilized to perform 1000 fps HSA, and has a 100-μm pixel pitch with a 7.5-cm x 5-cm field of view. The imaging ROI was localized on the aortic root region, where the outflow graft was anastomosed to the aorta. Imaging was performed using the x-ray source in the Canon-Toshiba Surginix

SXT 2000A Mobile C-Arm system (Canon Medical Systems USA Inc., Tustin, CA). The exposure duration was set at a continuous 1-second interval to ensure that a large number of image frames were available for analysis.

A programmable syringe injector (Legato 110, Cole Parmer, Vernon Hills, IL) was used to inject Ethiodol, a non-soluble iodine-based contrast media (Cerenovus, Miami, FL). Ethiodol breaks into small droplets after injection and has been used previously in neurovascular research applications, as well as hysterosalpingography and lymphography.[12] Ethiodol was chosen as the flow tracer in this study due to its tendency to form droplets (i.e., particles), which allows for in-vitro validation of both the optical flow and particle tracking algorithms used to study HSA sequences. A 5-French catheter (Vascular Solutions, Minneapolis, MN) was placed at the proximal end of the outflow graft to ensure that any visible flow patterns were due to the flow conditions within the phantom, as well as the vessel geometry. An Ethiodol volume of 3 mL was injected at a constant rate of 1.5 mL/second to ensure sufficient particle density within the lumen of the aorta and outflow graft anastomoses zone. Due to the low injection rate with respect to the flow through the outflow graft, the Ethiodol particles were assumed to have little inertia and act as a suitable flow tracer throughout the imaging ROI. The particle sizes are variable, but generally sub-millimeter in diameter and reliably tracked throughout the high-speed sequence.[16, 17]

Image Analysis: X-Ray Particle Image Velocimetry (X-PIV) Method

Tracking of the Ethiodol particles was performed using in-house software.[18] Ethiodol centroids are located in one frame and tracked through subsequent frames. The centroid locations can be further refined via the use of size and intensity thresholds. The change in centroid location frame-to-frame is then used to calculate the particle velocity, given the acquisition frame rate, magnification factor, and detector pixel size.

Image Analysis: Optical Flow Method (OFM)

Conventional optical flow methods (OFM) are based on measurement of the temporal change in image intensity. As defined by Horn and Schunck[19], by assuming small motion, a differential-equation algorithm can be used for calculation of the displacement vectors between frames of an image sequence. To better relate these changes in intensity to physical properties of fluid motion, the link between optical flow and fluid flow was established through the projection of the transport equations in three-dimensional space onto the image plane.[20, 21] This process yields image intensity changes related to a velocity field, such that the intensity changes are consistent with fluid behavior (Video S1). The OFM is used on the same Ethiodol particle sequence input to the X-PIV algorithm, but it should be noted that the method can also be used with conventional, soluble contrast media.[15] A high-resolution velocity distribution is obtained, where velocity vectors are calculated every 100 microns. A more detailed explanation of the OFM is provided in the online appendix.

Derivation of Shear Stress

LVAD-induced flow results in high spatial velocity gradients combined with an oscillating shear environment, leading to platelet activation.[22] These altered hemodynamics are implicated in thromboembolic complications, where prolonged platelet activation leads to

an enhancement in the aggregation of platelets, increasing the risk for thromboemboli formation.[23] As a surrogate for platelets, the shear stress experienced by the Ethiodol particles is investigated as an additional high-speed-derived metric. While the Ethiodol particles are larger than typical platelets, our capability to resolve particle motion is limited by the 100-micron pixel size of the detector. As a proof-of-concept, the shear stress accumulated by each particle was evaluated as a function of time in the flow within the detector FOV:

$$Accumulated \quad Shear = \int_{t_0}^{t} \tau(X(t'), \quad t')dt' \tag{1}$$

where τ is the instantaneous shear stress magnitude at time t' and $X(t')$ is the particle's location at that time. Over the 200-millisecond time interval of the trajectory with 1-millisecond sampling as in this study, the accumulated shear is calculated as:

$$Accumulated\ Shear = \sum_{n=1}^{200} \tau(n) \times 0.001\ Pa \cdot s \tag{2}$$

where n is the index for shear stress and τ is in units of Pa. The instantaneous shear stress is calculated by taking the spatial gradient of velocity at each particle centroid location, as tracked by the X-PIV algorithm.[16] These values can then be integrated along each trajectory to evaluate the total accumulated shear.

Computational Fluid Dynamics Simulation and Boundary Conditions

The aorta geometry, mesh, and flow simulation replicated a previously published computational study.[9] Mesh files were generated from the aortic arch with virtually anastomosed LVAD outflow grafts (ICEM, ANSYS Inc., Canonsburg, PA), containing between 1.7 and 2.9 million elements, depending on the configuration. This corresponded to an average element size of approximately 170 microns, which was downsampled in post-processing to match the resolution of our high-speed detector. The outflow graft was defined as the only inlet, and the great vessels (brachiocephalic, carotid, subclavian arteries) and descending aorta were all defined as outlets. A parabolic velocity profile was defined across each outflow graft cross-section, generating a mean flow rate of 5 L/min. All arterial walls were considered no-slip walls, and a zero-pressure gradient was assumed at each outlet. The blood material was defined as a Newtonian fluid with a density of 1060 kg/m^3 and viscosity of 0.0035 Pa-s.

Laminar, transient flow simulations were performed by numerically solving the incompressible Navier-Stokes equations in ANSYS Fluent (ANSYS Inc., Canonsburg, PA), assuming rigid walls. The time step was set at 1 millisecond, balancing both computational resources and simulation accuracy. Most importantly, this matches the temporal resolution of our high-speed detector, and is critical in evaluating the full capability of the high-speed method to provide flow details as an alternative to traditional computational simulations. Data was obtained over a total duration of 1 second to provide sufficient temporal resolution to resolve all unsteady motions in the flow. The convergence criteria was set to 1e-6

for continuity and momentum, and the SIMPLE scheme was implemented with a second order formulation. Additional information detailing the simulation of platelet particles for the same geometry is given in the previous publication of Aliseda et al.[9] For comparison with HSA velocimetry data, the 3D volume and corresponding velocity streamlines were co-registered to the HSA acquisition view.

Quantitative Comparison with CFD

Quantification of flow patterns was performed using a 1-millisecond sampling interval. For the X-PIV analysis, all trajectories were mapped over the 1-second interval, with over 100,000 velocity measurements calculated in the ascending aorta volume for each graft configuration. To better capture the comprehensive nature of the transient flow in the aorta with the OFM, pixelwise averages are performed over the 1-second interval to create temporally averaged velocity distributions, where velocity vectors were estimated at the resolution of 1 vector per 100 microns. 3D CFD streamlines are shown to give context to the flow patterns found throughout the depth of the ascending aorta and aortic root region, as well as enhancing our understanding of the projected angiographic flow patterns.

Results

High-Speed Image Sequences

High-resolution hemodynamic patterns of Ethiodol particles entering the aortic root region are shown in Videos 1 and 2. The high-velocity inflow jet from the 90-degree graft impinges on the contralateral wall of the ascending aorta: particles form recirculating eddies that move retrograde towards the outflow graft and form an isolated recirculation zone in the aortic root region. Comparatively, the Ethiodol particles in the 45-degree configuration experience less swirling motion after entering the aortic volume. Comparison of particle trajectory maps in Figure 3 clearly demonstrate the malignment of the inflow jet with the central aortic axis in the 90-degree graft configuration. From the high-speed sequence, particles exiting the shallower-angle graft experience smoother motions as they are transported downstream, while particles in the 90-degree model experience strong deflections and overall, more circuitous trajectories. Further, more particles appear to exit the Aries FOV towards the great vessels in the 45-degree configuration than in the 90-degree configuration.

Quantitative Comparison with CFD

A comparison of CFD and HSA is given in Figure 4 for both graft configurations. High-speed-derived velocity vectors are displayed with an 8×8 binning kernel for clarity. For both quantification methods, maximum projected velocities in each model were approximately 150 cm/second out of each graft, which subsequently decreased when entering the volume of the ascending aorta. Most significant in the high-speed distributions are the replication of the recirculation and stagnation regions in the CFD, such as those inferior to the 90-degree outflow graft which are formed as the high-velocity inflow jet impinges and splits on the contralateral wall. A secondary vortex-flow region is also present superior to the outflow graft. Lower-velocity streams are shown to split from the main jet in the 45-degree configuration, creating a larger recirculation region between the graft anastomosis and aortic root boundary. Through the CFD streamlines, we can confirm that for the 45-degree case

most flow streamlines move in the direction of the great vessels. Additional 2D velocity distributions derived from CFD are compared in the online appendix, including a depth-averaged velocity distribution, as well as a maximum intensity projection (MIP) of the 3D velocity distribution (Figure S1). These additional distributions assist in understanding the effect of integrating the particle motions at depth on velocity quantification in the imaging plane.

Paramount to quantification of high-resolution flow patterns is the capability to adequately capture the motion of the radiopaque tracer. A comparison with simulated frame rates is given in Figure 5 for the 90-degree model to illustrate the necessity of using 1000 fps for quantitative analysis: high-speed frames were retrospectively binned to generate simulated frame rates ranging from 25 fps, the near maximum for standard clinical angiography, to 500 fps. As seen in Figure 5A–D, at low acquisition frame rates the blurring of the Ethiodol media becomes substantial such that the individual particles appear to be continuous streams of contrast. X-PIV and OFM were performed on each dataset, and the velocity vector fields are shown in Figure 5E–H and 5I–L, respectively. Compared to the 1000 fps velocity distribution, qualitative and quantitative analysis of complex flow patterns below 500 fps, such as the two large vortices (red arrows) and flow impingement on the contralateral wall of the aorta (green arrows) cannot accurately quantified.

Quantitative Flow Analysis with HSA

Line profiles were drawn across each temporally averaged velocity distribution calculated by the OFM and are shown in Figure 6. Qualitative comparisons between the projected velocity maps indicate a non-homogeneous velocity distribution along the contralateral wall in the 90-degree model, where high-velocity streams ($V_{Average}$ = 86.6 cm/s) directly impinge on the vessel wall. Comparatively, the velocities reaching the wall in the 45-degree model are much lower ($V_{Average}$ = 16.6 cm/s). The percent reduction in velocity between the 90- and 45-degree configurations was approximately 81%. Similarly, velocities in the recirculation region across the line profile were reduced by 65% from the 90- ($V_{Average}$ = 54.8 cm/s) to 45-degree ($V_{Average}$ = 19.2 cm/s) graft.

Shear Stress

To demonstrate the high-speed capability of our HSA setup for shear stress calculation, the instantaneous and accumulated shear stress is calculated for several droplets: accumulated stress is calculated in the vicinity of the inflow jet and recirculation zone in the aortic root region over the trajectory length covered by a droplet for a duration of 200 milliseconds (Figure 7). Numerous deflections in droplet trajectories can be seen, particularly in the vicinity of the inflow jet. Of the particle trajectories shown in Figure 7, accumulated shear stress reached upwards of 5.0 Pa-ms within the detector FOV, where droplets tend to experience higher shear more often in the vicinity of the inflow jet ($P1_{90}$=1.9 Pa-ms, $P2_{90}$=2.9 Pa-ms, $P1_{45}$=5.0 Pa-ms, $P2_{45}$=5.0 Pa-ms). The often-cited threshold for platelet activation is 3.5 Pa-s[23]; previously published findings by Aliseda et al. investigated the accumulated shear stress of over 150,000 platelets given identical geometries and flow conditions, where a significant number of droplets had a high probability of accumulated

shear between 0.5 and 2 Pa-s.[9] Therefore, we could expect to see shear activation occurring in the vicinity of the aorta under the abnormal flow conditions in either graft configuration.

Discussion

In this work, a novel application of 1000 fps HSA to assess hemodynamic differences between two LVAD outflow graft configurations is presented. The authors hypothesize that the HSA technology would make detailed hemodynamic assessment possible over a range of vascular pathologies, where the capability to derive meaningful quantitative flow information in a diagnostic imaging setting would be of value. By confirming the results of prior LVAD research, the authors believe that there are grounds for translation of this quantitative imaging approach to in-vivo use, where we can directly image the true physiologic flow at a fraction of the time needed for computational simulations. The authors postulate that this method would be of significance in a number of clinical scenarios, such as vascular interventions, where immediate adjustments to the flow and flow-modifying devices can be of potential use in avoiding complications.[24] This can span both the cardio- and neurovascular space, where motion reduction measures and quantification of actual flow parameters are both of interest and value clinically.

Because assumptions are made in the CFD simulation with regards to the flow boundary conditions, X-PIV was also performed to support the validity of the OFM in characterizing the in-vitro flow environment. In fact, optical Particle Image Velocimetry (PIV) is a widely accepted method of in-vitro velocimetry, and has been used to perform velocimetry in transparent LVAD models.[25] The high velocity gradients, jet impingement, and redirection of flow in the ascending aortic region were comprehensively captured. Velocity distributions in the ascending aorta were in overall good agreement between both HSA methods, where the same image sequence was used in both methods. Importantly, when both algorithms were used on simulated frame rates ranging from 25 – 500 fps, the capability to visualize and quantify complex flow patterns within the 90-degree model was compromised. This phenomenon is in line with previous findings, where the magnitude and spatial distribution of velocity increasingly deviates from the 1000 fps standard due to blurring of the contrast media, even when lower velocities are expected.[15]

In alignment with the CFD results, significant findings include the large recirculation region found within both graft configurations: the trapping of Ethiodol droplets in these recirculation zones leads to increased residence time in the aortic arch before moving to the distal circulation, where increased residence time is an essential step towards agglomeration after flow-induced platelet activation. While the recirculation region inferior to the anastomosis zone in the 45-degree graft configuration was comparatively larger than that of the 90-degree, the velocities were overall lower in this region. Further, the motion in this region was less erratic, due to the improvement in alignment of the momentum of the inflow jet with the central axis of the aorta. By comparison, multiple high-speed swirls were present in the 90-degree configuration, breaking off from the inflow jet as it impinges on the contralateral wall of the aorta. The isolated stagnation region that forms as particles circulate in the aortic root creates the potential for agglomeration after an activation event.[9, 26–28] It should be noted that these flow patterns may also vary depending on the length of the

proximal aorta: variation in the length distal to the anastomoses site (towards the arch vessels) may give rise to secondary flow patterns such as vortices and local recirculation regions for larger distances. However, this is also strongly influenced by the anastomoses angle and would necessitate a detailed follow-up analysis.

The decision to evaluate both a clinically desirable, shallower anastomosis angle and the unpreferred, large anastomosis angle was twofold: firstly, to provide a comparison of the two outflow graft conditions discussed in the previous study by Aliseda et al. Secondly, and more importantly, to demonstrate the full capability of the high-speed method in evaluating adverse hemodynamics: in the case of the LVAD, it was important to span the range of possible outflow graft anastomoses configurations. Recent studies have demonstrated the potential harmful effects of a 90-degree (or greater) anastomosis angle, and its effects on aortic regurgitation, demonstrating clinical relevancy of evaluating such configurations.[29] Confirming the presence of additional effects from large anastomosis angles, or outflow graft obstructions such as kinking in the proximal graft, would be of clinical interest and could be addressed in future works.[30, 31]

Platelets are activated by high shear rate, and the level of activation is proportionally related to the time exposure, accumulating with circulation of the LVAD pump.[32] If we conceptualize the Ethiodol particle-droplets as a surrogate for blood-suspended particles, the particles in either graft configuration experience sharp velocity gradients before moving out of the aortic root region and into systemic circulation, as the majority need to pass through the high-velocity inflow jet. The few measured particle trajectories used for calculation of shear illustrate the capability of the high-speed method in calculating additional parameters derived from velocity, namely heterogeneous instantaneous shear exposure. It should be noted that the values of shear calculated in this exercise are likely under-representing the actual shear, as the out-of-plane gradients are not fully resolved with planar angiography. Further, only a short duration of 200 milliseconds was used for calculation which is not indicative of the overall flow environment for longer times: however, if we assume the shear exposure behavior is repeated for 10 cardiac cycles, our integral shear estimate is then over 0.25 Pa-s, in line with previous computational studies even without taking into account the under-estimation.[7] It is worth noting that recent studies have found the temporal oscillations in shear stress to be important mechanisms in platelet activation, particularly for the case of blood recirculating devices: therefore, the capability to resolve heterogeneous shear exposure through HSA warrants further investigation.[33] The current in-vitro study, at present, was limited to exposure times of less than 1 second at the highest frame rate of 1000 fps, and thus, can only capture particles within a smaller temporal window. Therefore, analysis of residence time was omitted. However, the image-based analysis confirms previous findings that both LVAD graft configurations create a hemodynamic environment that is likely predisposed to platelet activation and/or endothelial damage, which increases the risk of stroke.[34]

Without the aortic valve opening, the droplets trapped in the isolated recirculation zone would be more susceptible to conglomeration and potentially influence aortic valve regurgitation over time.[35] Several research efforts have found that a large angle between the LVAD outflow graft and proximal ascending aorta might increase the retrograde blood flow

over the aortic valve.[36, 37] These findings set the motivation for additional investigations into the effect of aortic valve opening on the hemodynamics within the aortic root region.

Study Limitations

There are inherent limitations in using planar acquisitions to characterize the flow in the aorta after LVAD implantation, due to the highly complex 3D nature of the flow. X-PIV and OFM extract the physical modulation of attenuated Ethiodol projections over the sequence, where only 2D velocity distributions can be assessed presently. This extends to shear stress estimates as well, which are further limited to the detector FOV. Current research efforts include the development of a biplane HSA system, where depth-dependent flow information could be better recovered by combining velocity distributions from two planes.[38]

Additionally, the fluid-tracer used in this experiment is not safe for in-patient diagnostic use. Ethiodol was chosen in this instance due to its non-soluble droplet properties, which is useful in calibrating the optical flow method with another in-vitro method, like X-PIV, when high velocities and erratic flow patterns are expected. Traditional water-soluble contrast media would need to be used in a clinical setting, which is still applicable to the OFM and has been evaluated extensively in the neurovascular domain.[39, 40]

In practice, LVAD's are used with variable waveforms, moving away from the constant 5 L/min used in this study. The objective of this study was to directly compare in-vitro high-speed angiography with previously published computational analysis, which utilized a constant flow rate. The timing of the contrast injection with respect to the flow cycle is crucial in temporally synchronizing the high-speed flow quantification with the simulation. Currently, an updated system is being implemented which synchronizes the contrast injection, flow waveform, and x-ray detector acquisition.[38] This would enable follow-up studies with more realistic waveforms in the future, including further exploration of rotor speed modulation, which has been shown to provide a contributory effect in terms of platelet activation and overall LVAD thrombogenicity.[41]

Conclusions

This investigation presents a novel in-vitro velocimetry method using 1000 fps high-speed x-ray angiography, applied to the analysis of the hemodynamic differences between two LVAD outflow graft configurations. HSA-derived metrics provide a good representation of the significant flow patterns seen in corresponding CFD simulations, such as vortices and sharp velocity gradients. The results of this study demonstrate the potential advantage of leveraging high-speed imaging to capturing fast moving blood flow phenomenon.

Supplementary Material

Refer to Web version on PubMed Central for supplementary material.

Acknowledgements

This work was supported by NIH Grant 1R01EB030092 and Canon Inc.

Glossary of Abbreviations:

2D	2-dimensional
3D	3-dimensional
CFD	computational fluid dynamics
CTA	computed tomography angiography
FPD	flat panel detector
HF	heart failure
HSA	high-speed angiography
LVAD	left ventricular assist device
MIP	maximum intensity projection
PCD	photon-counting detector
ROI	region of interest

References

1. Nixon AM, Gunel M, Sumpio BE. The critical role of hemodynamics in the development of cerebral vascular disease: A review. Journal of Neurosurgery JNS112(6):1240–1253. 2010.
2. Hsu S, Fang JC, Borlaug BA. Hemodynamics for the Heart Failure Clinician: A State-of-the-Art Review. J Card Fail28(1):133–148. 2022. [PubMed: 34389460]
3. Willey JZ, Boehme AK, Castagna F, et al. Hypertension and Stroke in Patients with Left Ventricular Assist Devices (LVADs). Curr Hypertens Rep18(2):12. 2016. [PubMed: 26781252]
4. Morgan JA, Brewer RJ, Nemeh HW, et al. Stroke while on long-term left ventricular assist device support: incidence, outcome, and predictors. ASAIO J60(3):284–289. 2014. [PubMed: 24625532]
5. Long B, Robertson J, Koyfman A, Brady W. Left ventricular assist devices and their complications: A review for emergency clinicians. Am J Emerg Med37(8):1562–1570. 2019. [PubMed: 31072684]
6. Perna E, Wettersten N. Evaluation and Management of LVAD Complications. Case-Based Device Therapy for Heart Failure Cham: Springer International Publishing. 2021.
7. Acharya D, Loyaga-Rendon R, Morgan CJ, et al. INTERMACS Analysis of Stroke During Support With Continuous-Flow Left Ventricular Assist Devices: Risk Factors and Outcomes. JACC Heart Fail5(10):703–711. 2017. [PubMed: 28958345]
8. Inci G, Sorguven E. Effect of LVAD outlet graft anastomosis angle on the aortic valve, wall, and flow. ASAIO J58(4):373–381. 2012. [PubMed: 22739783]
9. Aliseda A, Chivukula VK, McGah P, et al. LVAD Outflow Graft Angle and Thrombosis Risk. ASAIO J63(1):14–23. 2017. [PubMed: 28033200]
10. Karmonik C, Partovi S, Loebe M, et al. Influence of LVAD cannula outflow tract location on hemodynamics in the ascending aorta: a patient-specific computational fluid dynamics approach. ASAIO J58(6):562–567. 2012. [PubMed: 23013842]
11. Chivukula VK, Beckman JA, Li S, et al. Left Ventricular Assist Device Inflow Cannula Insertion Depth Influences Thrombosis Risk. ASAIO J66(7):766–773. 2020. [PubMed: 31453832]
12. Chivukula VK, Beckman JA, Prisco AR, et al. Small Left Ventricular Size Is an Independent Risk Factor for Ventricular Assist Device Thrombosis. ASAIO J65(2):152–159. 2019. [PubMed: 29677037]

13. Flores AS, Essandoh M, Yerington GC, et al. Echocardiographic assessment for ventricular assist device placement. J Thorac Dis7(12):2139–2150. 2015. [PubMed: 26793334]
14. Shroff GS, Ocazionez D, Akkanti B, et al. CT Imaging of Complications Associated with Continuous-Flow Left Ventricular Assist Devices (LVADs). Semin Ultrasound CT MR38(6):616–628. 2017. [PubMed: 29179901]
15. Shields A, Nagesh SVS, Ionita C, Bednarek DR, Rudin S. Evaluation of methods to derive blood flow velocity from 1000 fps high-speed angiographic sequences (HSA) using optical flow (OF) and computational fluid dynamics (CFD). Proc SPIE Int Soc Opt Eng11595. 2021.
16. Krebs J, Shields A, Sharma A, et al. Initial investigations of x-ray particle imaging velocimetry (X-PIV) in 3D printed phantoms using 1000 fps High-Speed Angiography (HSA). SPIE Medical Imaging11317. 2020.
17. Shields A, Setlur Nagesh SV, Ionita C, Bednarek DR, Rudin S. Characterization of velocity patterns produced by pulsatile and constant flows using 1000 fps high-speed angiography (HSA). Proc SPIE Int Soc Opt Eng11600. 2021.
18. Allan D, Casewell T, Keim N,C, van der Wel CM. trackpy: Trackpy v0.4.1 2018.
19. Horn BKP, Schunck BG. Determining Optical-Flow. Artif Intell17(1–3):185–203. 1981.
20. Wildes RP, Amabile MJ, Lanzillotto AM, Leu TS. Recovering estimates of fluid flow from image sequence data. Comput Vis Image Und80(2):246–266. 2000.
21. Liu TS, Shen LX. Fluid flow and optical flow. J Fluid Mech614:253–291. 2008.
22. Mehra MR, Stewart GC, Uber PA. The vexing problem of thrombosis in long-term mechanical circulatory support. J Heart Lung Transplant33(1):1–11. 2014. [PubMed: 24418729]
23. Hellums JD, Peterson DM, Stathopoulos NA, Moake JL, Giorgio TD. Studies on the Mechanisms of Shear-Induced Platelet Activation1987; Berlin, Heidelberg: Springer Berlin Heidelberg.
24. Nagesh SVS, Shields A, Wu X, et al. Use of 1000fps High Speed X-ray Angiography (HSAngio) to quantify differences in flow diversion effects of three stents with different coverage densities in a cerebral aneurysm invitro model. Proc SPIE Int Soc Opt Eng12031. 2022.
25. Scardulla F, Bellavia D, D'Acquisto L, Raffa GM, Pasta S. Particle image velocimetry study of the celiac trunk hemodynamic induced by continuous-flow left ventricular assist device. Med Eng Phys.47:47–54. 2017. [PubMed: 28709930]
26. Aliseda A, Chivukula VK, Chassagne F, et al. Abstract 13317: Optimization of Left Ventricular Assist Device Therapy: A Combined in vitro and in silico Strategy to Reduce Thromboembolic Adverse Events via Evidence-Based Surgical Configuration and Medical Management. Circulation144(Suppl_1):A13317–A13317. 2021.
27. Chassagne F, Miramontes M, Chivukula VK, et al. In Vitro Investigation of the Effect of Left Ventricular Assist Device Speed and Pulsatility Mode on Intraventricular Hemodynamics. Ann Biomed Eng49(5):1318–1332. 2021. [PubMed: 33128182]
28. Selmi M, Chiu W-C, Chivukula VK, et al. Blood damage in Left Ventricular Assist Devices: Pump thrombosis or system thrombosis? The International Journal of Artificial Organs42(3):113–124. 2019. [PubMed: 30354870]
29. Iizuka K, Nishinaka T, Ichihara Y, Miyamoto T, Yamazaki K. Outflow graft anastomosis site design could be correlated to aortic valve regurgitation under left ventricular assist device support. J Artif Organs21(2):150–155. 2018. [PubMed: 29164425]
30. Trankle CR, Grizzard JD, Shah KB, et al. Left Ventricular Assist Device Outflow Graft Compression: Incidence, Clinical Associations and Potential Etiologies. J Card Fail25(7):545–552. 2019. [PubMed: 31085224]
31. Nathan S, Ghotra AS, Rajagopal K, et al. Left Ventricular Assist Device Outflow Graft Obstruction: A Case Series. ASAIO J66(6):657–662. 2020. [PubMed: 31425271]
32. Bluestein D, Chandran KB, Manning KB. Towards non-thrombogenic performance of blood recirculating devices. Ann Biomed Eng38(3):1236–1256. 2010. [PubMed: 20131098]
33. Consolo F, Sheriff J, Gorla S, et al. High Frequency Components of Hemodynamic Shear Stress Profiles are a Major Determinant of Shear-Mediated Platelet Activation in Therapeutic Blood Recirculating Devices. Sci Rep7(1):4994. 2017. [PubMed: 28694489]

34. Dolan JM, Meng H, Singh S, Paluch R, Kolega J. High fluid shear stress and spatial shear stress gradients affect endothelial proliferation, survival, and alignment. Ann Biomed Eng39(6):1620–1631. 2011. [PubMed: 21312062]

35. Aggarwal A, Raghuvir R, Eryazici P, et al. The development of aortic insufficiency in continuous-flow left ventricular assist device-supported patients. Ann Thorac Surg95(2):493–498. 2013. [PubMed: 23245444]

36. Pak SW, Uriel N, Takayama H, et al. Prevalence of de novo aortic insufficiency during long-term support with left ventricular assist devices. J Heart Lung Transplant29(10):1172–1176. 2010. [PubMed: 20619680]

37. DiGiorgi PL, Smith DL, Naka Y, Oz MC. In vitro characterization of aortic retrograde and antegrade flow from pulsatile and non-pulsatile ventricular assist devices. J Heart Lung Transplant23(2):186–192. 2004. [PubMed: 14761766]

38. Setlur Nagesh SV, Shields A, Wu X, et al. Simultaneous biplane high speed 1000 fps x-ray angiography (HSAngio). SPIE 2022.

39. Brina O, Ouared R, Bonnefous O, et al. Intra-aneurysmal flow patterns: illustrative comparison among digital subtraction angiography, optical flow, and computational fluid dynamics. AJNR Am J Neuroradiol35(12):2348–2353. 2014. [PubMed: 25082824]

40. Yang Z, Yu H, Huang GP, Ludwig B. Divergence Compensatory Optical Flow Method for Blood Velocimetry. J Biomech Eng139(6). 2017.

41. Boraschi A, Bozzi S, Thamsen B, et al. Thrombotic Risk of Rotor Speed Modulation Regimes of Contemporary Centrifugal Continuous-flow Left Ventricular Assist Devices. ASAIO J67(7):737–745. 2021. [PubMed: 33074865]

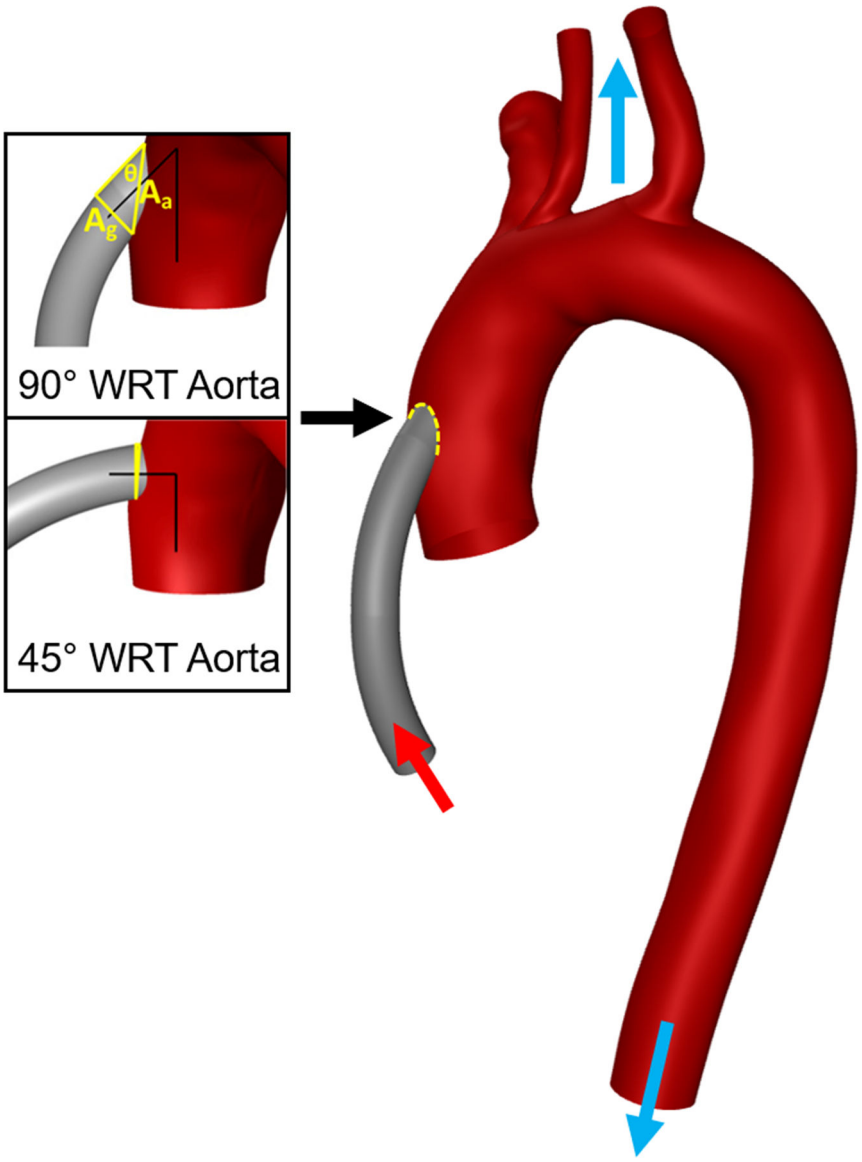

Figure 1. 3D LVAD Model:
Left-Ventricular Assist Device (LVAD) outflow graft configurations at 90- and 45-degrees with respect to the central aortic axis. The red arrow indicates the inflow direction, whereas the blue arrows indicate the outflow.

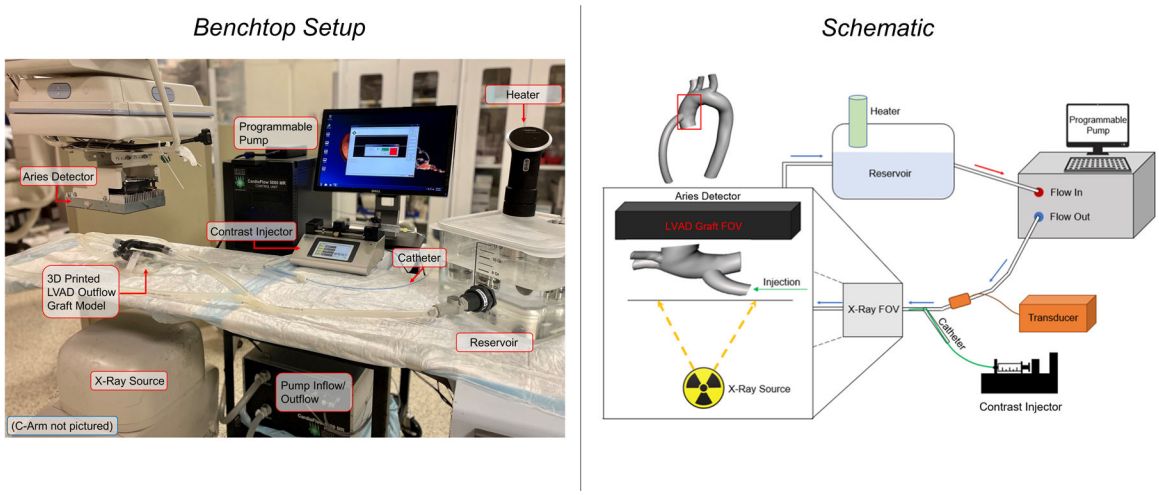

Figure 2. In-Vitro Flow Experiment:

Left) Benchtop flow loop mimicking 5 L/min flow through each Left-Ventricular Assist Device (LVAD) outflow graft. Not all components are shown for clarity. Right) Schematic including all flow loop components.

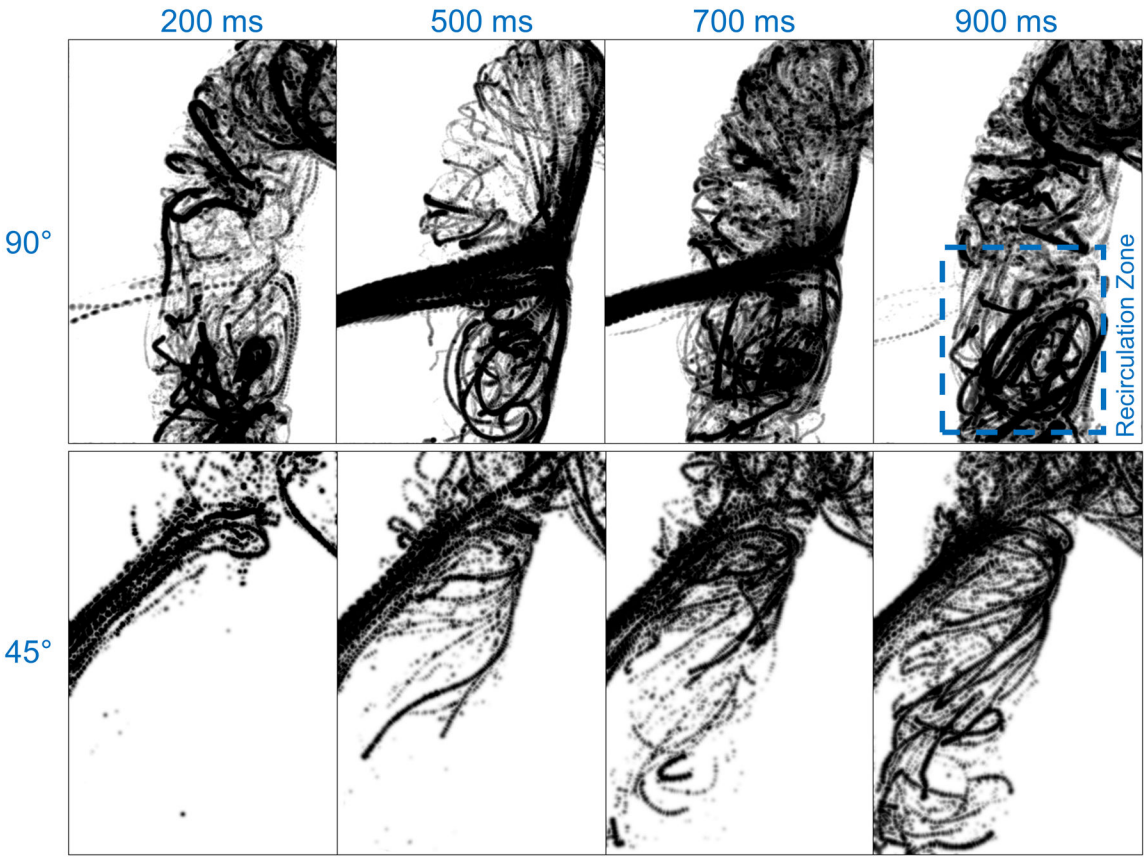

Figure 3. Ethiodol Trajectory Maps:

Individual 1-ms Ethiodol images are summed together in 100-frame increments to produce trajectory images for the 90-degree (top row) and 45-degree (bottom row) graft configurations.

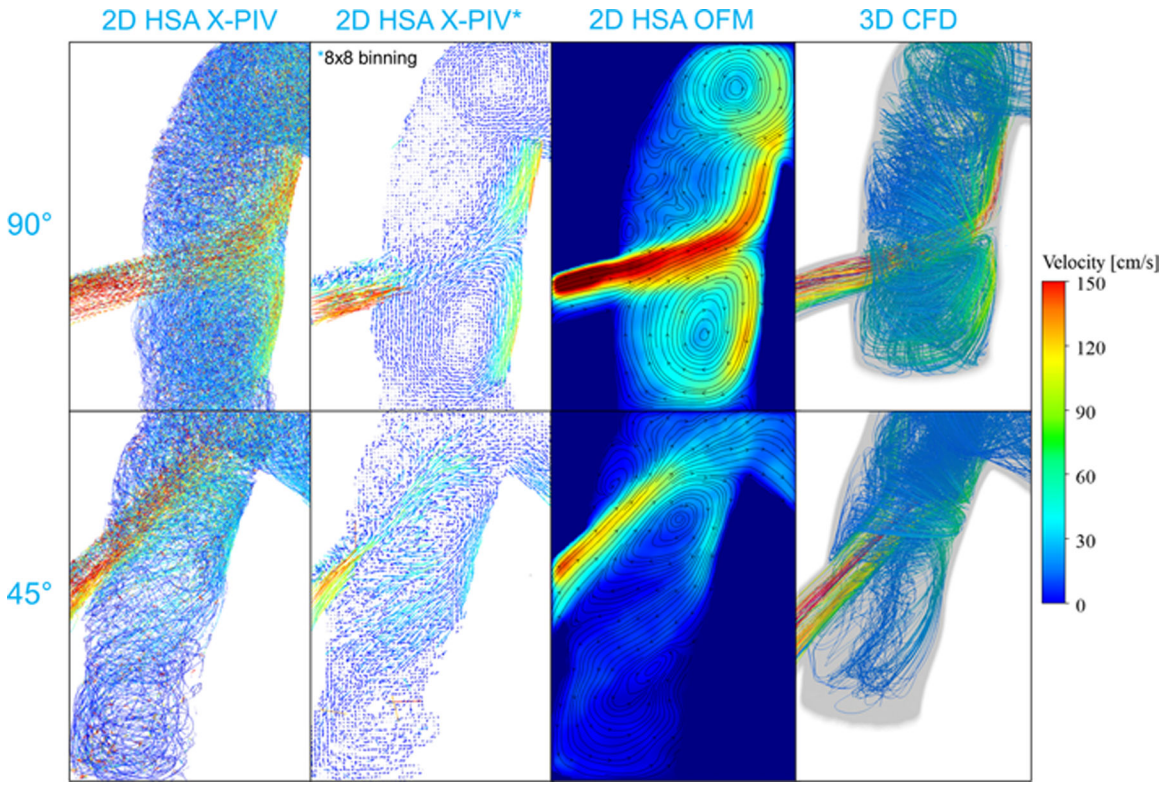

Figure 4. Projected Velocity Distributions from HSA:
Quantitative comparisons between temporally-averaged 2D High-Speed Angiography (HSA)-derived streamlines and temporally-averaged 3D computational fluid dynamics (CFD)-derived streamlines show good agreement between velocimetry results, as well as significant flow structures such as recirculation vortices and the splitting of the inflow jet throughout the ascending aorta.

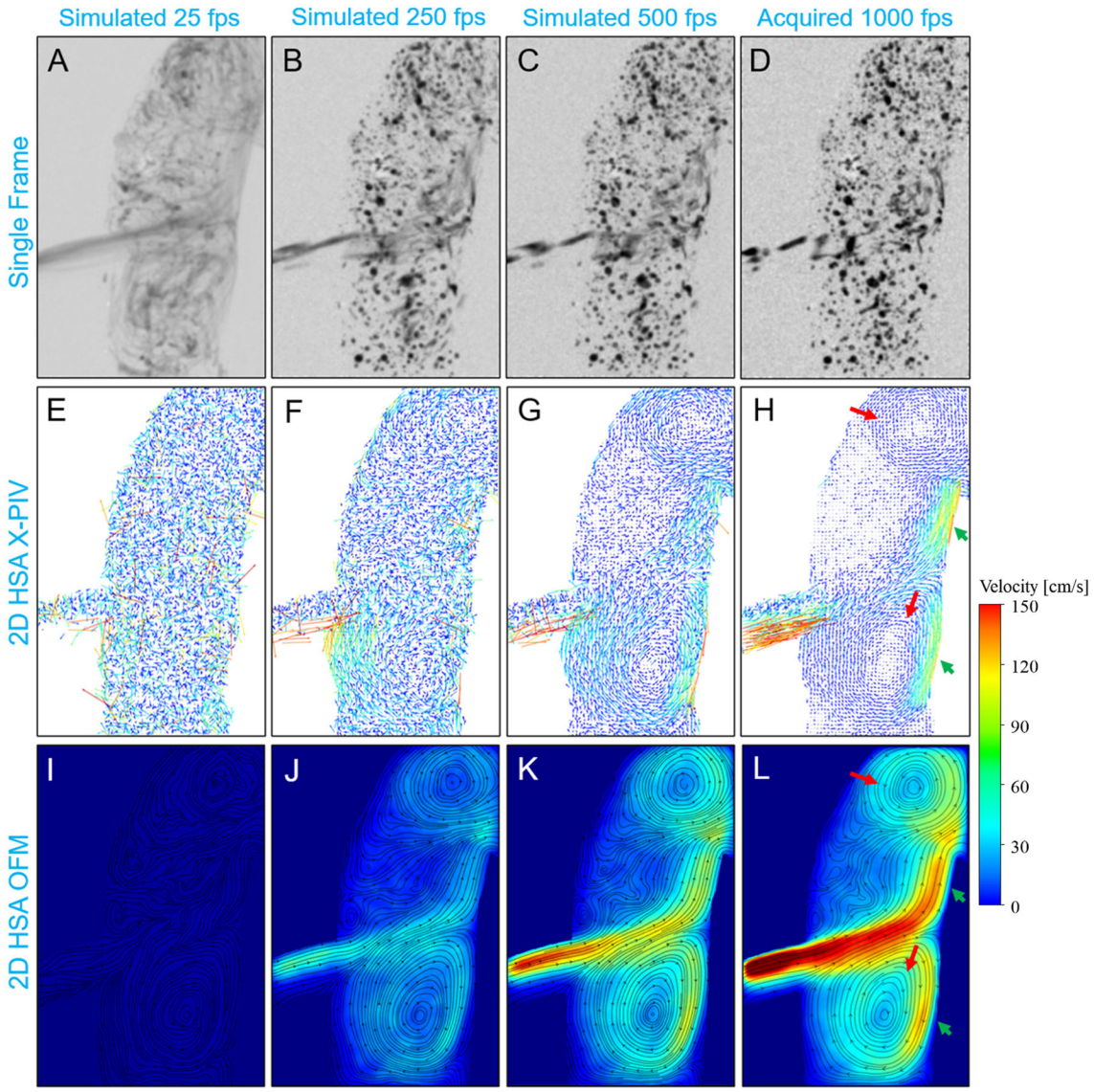

Figure 5. Simulated Frame Rates:

The 1000 fps acquisition was retrospectively binned to simulate lower frame rates (25, 250, 500 fps). The blurring of the Ethiodol particles becomes evident at lower frame rates and can degrade quantitative velocity analysis as shown by the corresponding X-PIV and OFM velocity distributions. X-PIV vectors are displayed with an 8×8 binning kernel for clarity.

Figure 6. Line Profile Analysis from HSA:

Line profiles index the temporally-averaged velocity distribution obtained with the Optical Flow Method (OFM) (dashed white lines indicate line profile location in each model) for velocity vectors calculated at a resolution of 1 vector per pixel.

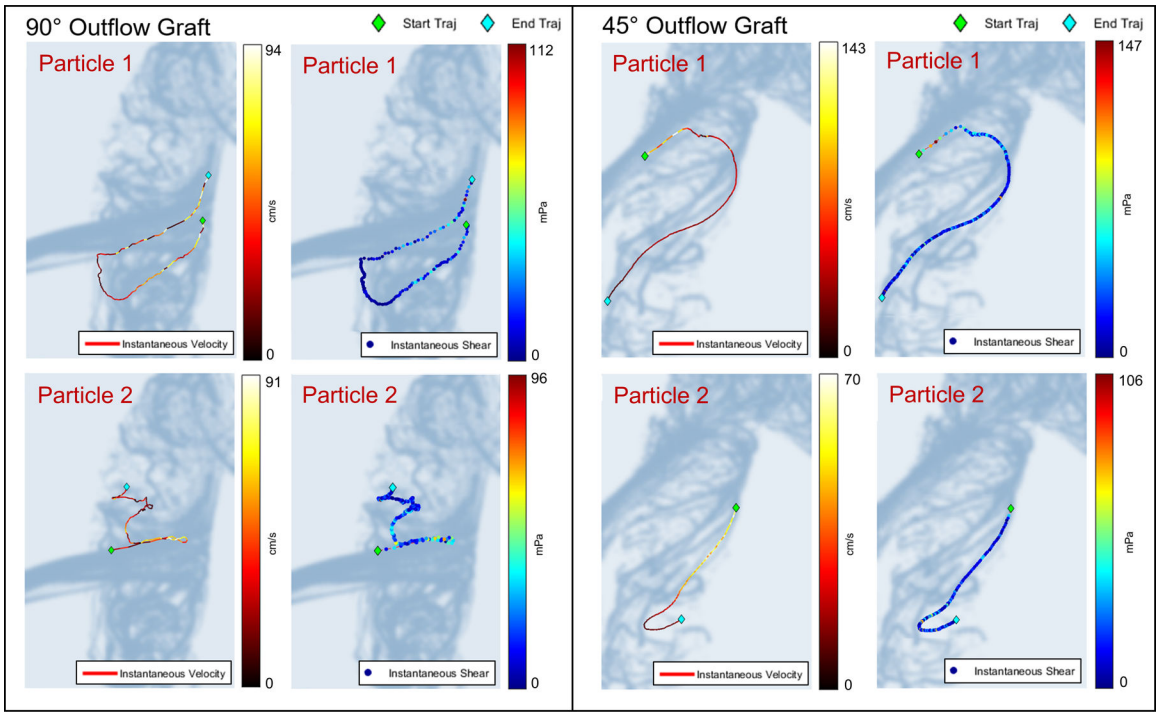

Figure 7. Shear Stress Estimation from HSA:

Two droplet trajectories are shown in each graft configuration, and instantaneous shear exposure is estimated on a 1-millisecond basis for a total duration of 200 milliseconds. Both instantaneous velocity and shear stress are plotted, where the colorbars indicate magnitude (note changing scale).

Video 1: Video 1. HSA in the 90-Degree Outflow Graft Configuration:
1000 fps Ethiodol injection from the 90-degree graft configuration into the aorta volume (playback 25 fps).

Video 2: Video 2. HSA in the 45-Degree Outflow Graft Configuration:
1000 fps Ethiodol injection from the 45-degree graft configuration into the aorta volume (playback 25 fps).